Electronic Supplementary Material (ESI) for Metallomics.


# Studies of copper trafficking in a mouse model of Alzheimer's disease by positron emission tomography using $^{64}$Cu acetate and $^{64}$CuGTSM.

Erica M. Andreozzi, Julia Baguña Torres, Kavitha Sunassee, Joel Dunn, Simon Walker-Samuel, Istvan Szanda and Philip J. Blower[1]
*Division of Imaging Sciences, Kings College London, St. Thomas Hospital, London, United Kingdom*
*UCL Centre for Advanced Biomedical Imaging, Division of Medicine, London, United Kingdom*

## Supplemental Data:

### *Materials and Methods*

### Radiolabeling of GTSM with $^{64}$Cu

$^{64}CuCl_2$ was initially buffered with a 3 M solution of sodium acetate to pH 6. To this 10 µL of a 1 mg/mL solution of GTSM ligand in dimethyl sulfoxide (DMSO) were added. The reaction mixture was vortexed for 1 minute and allowed to stand at room temperature for 5-10 minutes. The resulting $^{64}$CuGTSM solution was then loaded onto a $C_{18}$ Sep-Pak cartridge (previously conditioned with ethanol and water). The sample was washed though with water (5 mL) and finally eluted in ethanol (2 mL). The initial 0.5 mL ethanol fraction was discarded, the following 20 drops of ethanol, containing the purified $^{64}$CuGTSM complex, were collected and the remaining fraction was discarded. RadioTLC analysis of the radiolabelled complex was performed before and after purification ($R_f$ = 0.31, RCP≥ 95 %). $^{64}$CuGTSM in ethanol was then concentrated to ≤ 10 % of the total injection volume (< 200 µL) and reconstituted with sterile 0.9 % saline solution.

### Colour scaling for PET image display

All PET images were displayed as a %ID/g map, and the min/max values of this scaling were normalized for injected dose (ID). We use the following formula to calculate the appropriate Min/Max value (X) to input for the desired %ID/g:

$$X = [(\text{Desired \%ID/g}) \times ID \times \text{voxel volume}] / 100{,}000$$

where ID is the injected dose measured from the whole-body ROI (excluding the tail) at the time of injection, and 100,000 is a conversion factor (100 to convert the %ID/g to a percentage and 1000 to convert the volume of a voxel (0.016 $mm^3$) to grams based on water density of 1 g/mL). This formula calculates the uptake value that corresponds to the desired %ID/g value based on the ID and the gram value associated with the volume of a single voxel. In this way, all the images are normalized to display min/max corresponding to the same %ID/g.

**Mouse Brain Atlas for PET Quantification**

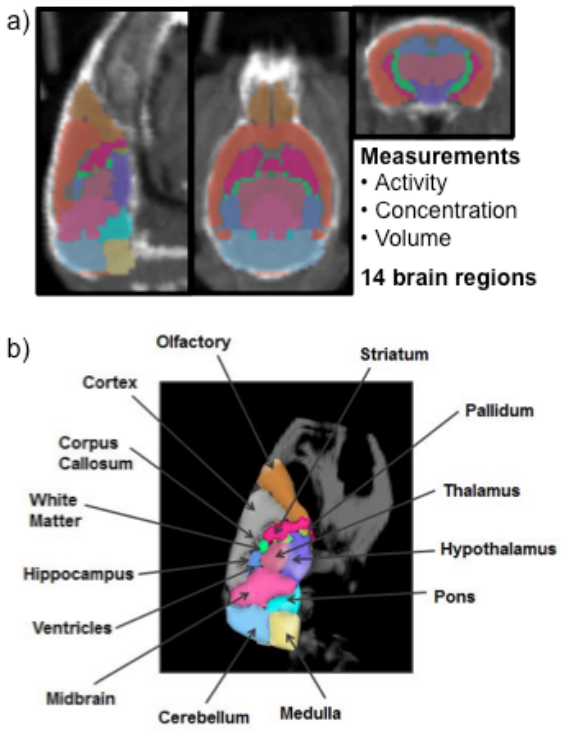


**Fig. S1**. a) Sagittal (left), coronal (middle) and axial (right) views of 3D mouse brain atlas. b) Sagittal view of the 3D mouse brain atlas, labelled with all 14 brain regions

## Quantification of co-registered autoradiography and histology images

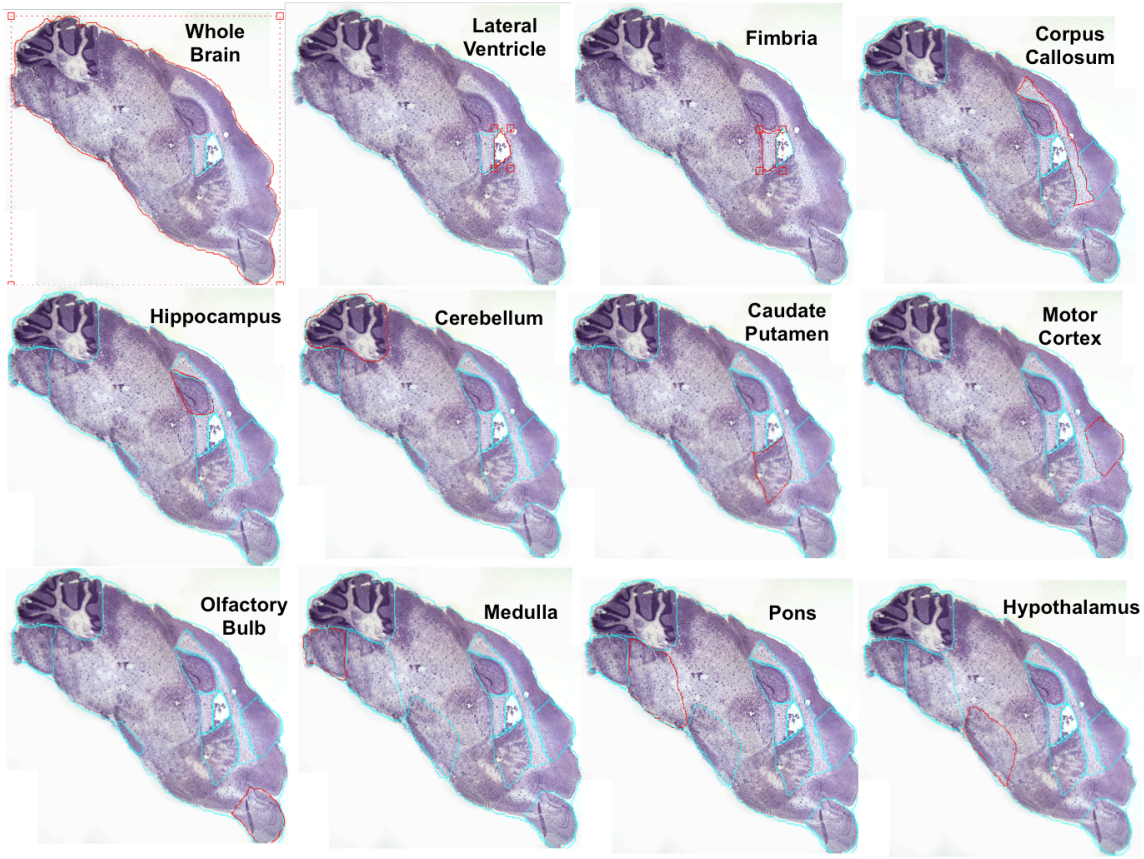


**Fig. S2**. Representative images depicting the specific brain regions (whole brain, lateral ventricle, fimbria, corpus callosum, hippocampus, cerebellum, caudate putamen, motor cortex, olfactory bulb, medulla, pons, and hypothalamus), outlined in red, for quantification of $^{64}$Cu signal in brain autoradiographs via manual region-of-interest (ROI) analysis using the specified in-house LDL software.

In order to verify the anatomical origin of the focal accumulations of $^{64}$Cu observed in/around the $^{64}$Cu-acetate autoradiographs, we used in-house software (PhosphorCount) in conjunction with Interactive Data Language (IDL, Boulder, CO) software to co-register autoradiography and histology images generated from the same brain tissue slices. Manual co-registration results in an overlay image (right) with green, monochomatic color scaling (autoradiograph signal intensity) superimposed on a photomicrograph of a haematoxylin stained section (Fig 6 and 8). This type of overlay image enabled us to draw accurate regions of interest (ROIs) in the distinct brain regions outlined by the haematoxylin stain, and then verify our ROI geometries and manual co-registration using the automated co-registration provided by the program. In all circumstances, we ensured that the manual overlay closely matched the objective overlay. This validated the results from our autoradiographic ROI analysis, and provided additional evidence that the regions of high $^{64}$Cu uptake in the case of $^{64}$Cu-acetate were indeed in and around the ventricular compartments.

***Results***

**Whole Body PET Biodistribution of $^{64}$Cu-Acetate and $^{64}$Cu-GTSM**

a)

| | 30 min | | 24 h | |
|---|---|---|---|---|
| | $^{64}$Cu-Acetate | $^{64}$Cu-GTSM | $^{64}$Cu-Acetate | $^{64}$Cu-GTSM |
| Heart | 3.49 ± 0.51 | 29.84 ± 3.87 | 2.45 ± 0.57 | 12.92 ± 1.85 |
| Lungs | 3.25 ± 1.05 | 20.20 ± 5.93 | 2.65 ± 0.47 | 5.88 ± 1.88 |
| Liver | 7.44 ± 1.46 | 15.16 ± 5.28 | 6.26 ± 0.82 | 8.10 ± 1.66 |
| Kidney | 21.90 ± 2.74 | 17.31 ± 3.76 | 18.62 ± 3.69 | 18.60 ± 3.71 |
| Brain | 0.73 ± 0.03 | 5.57 ± 0.77 | 0.76 ± 0.03 | 5.45 ± 0.75 |
| Spine | 1.02 ± 0.09 | 4.03 ± 0.46 | 0.98 ± 0.04 | 3.76 ± 0.31 |

b)

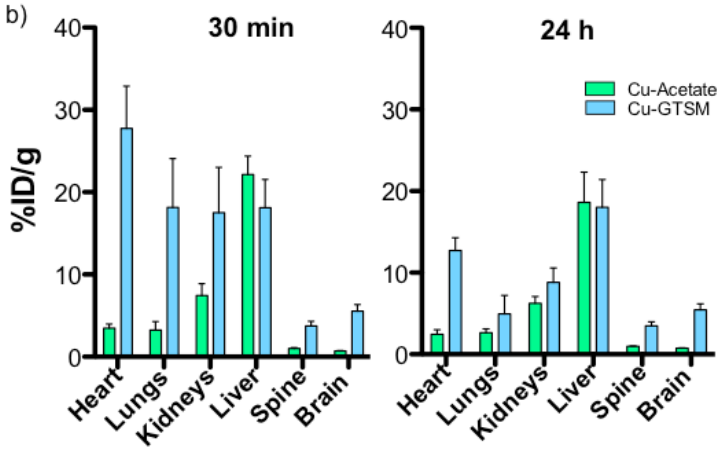


**Fig. S3**. Table (a) and corresponding bar charts (b) of values representing the *in vivo* distribution of $^{64}$Cu uptake (%ID/g) in 6-8-month-old C57BL6J mice at 30 min and 24 h post-injection of $^{64}$Cu-acetate (green) and $^{64}$CuGTSM (blue) derived from manual ROI analysis of PET. Data are mean (n=4 for $^{64}$Cu-acetate mice; n=6 for $^{64}$Cu-GTSM) ± SD.

**Whole Body PET Biodistribution of $^{64}$Cu-Acetate and $^{64}$Cu-GTSM: Individual Animal Time-Activity Relationships in Key Organs**

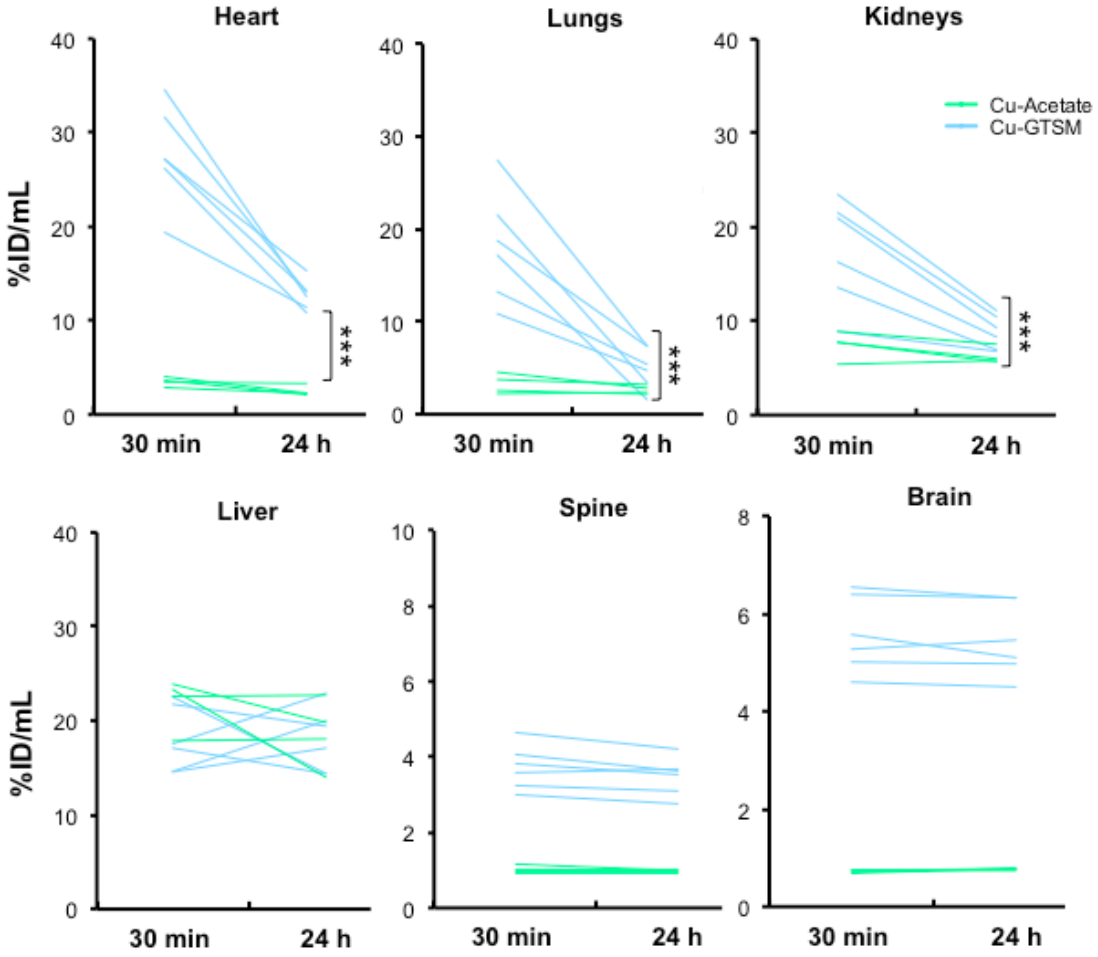


**Fig. S4**. Individual changes in activity concentration between 30 min and 24 h (%ID/mL) in major organs (heart, lungs, kidney, liver, brain, and spinal cord) following administration of $^{64}$Cu-GTSM (blue) and $^{64}$Cu-acetate (green). The uptake of $^{64}$Cu in all organs except liver (and blood, data not shown) is significantly higher ($p<0.001$) for $^{64}$Cu-GTSM than $^{64}$Cu-acetate at both 30 min and 24 h. $^{64}$Cu-GTSM clearance (30 min to 24) is only significant for heart, lungs, and kidney. There was no significant clearance of $^{64}$Cu-acetate from any of the organs between 30 min and 24 h. Each line represents a single animal. Data are n=4 for $^{64}$Cu-acetate and n=6 for $^{64}$Cu-GTSM.

**Brain Biodistribution of $^{64}$Cu-Acetate and $^{64}$Cu-GTSM: %ID/mL of Individual Brain Regions**

| | 30 min | | 24 h | |
|---|---|---|---|---|
| | $^{64}$Cu-Acetate | $^{64}$Cu-GTSM | $^{64}$Cu-Acetate | $^{64}$Cu-GTSM |
| Medulla | 0.98 ± 0.04 | 5.65 ± 0.78 | 0.81 ± 0.09 | 5.30 ± 0.70 |
| Cerebellum | 0.96 ± 0.07 | 5.56 ± 0.71 | 0.79 ± 0.06 | 5.16 ± 0.53 |
| Midbrain | 0.37 ± 0.05 | 6.69 ± 1.12 | 0.67 ± 0.03 | 6.90 ± 1.06 |
| Pons | 0.63 ± 0.12 | 5.76 ± 0.92 | 0.81 ± 0.05 | 5.96 ± 1.42 |
| Cortex | 0.71 ± 0.02 | 4.98 ± 0.76 | 0.61 ± 0.05 | 4.83 ± 0.65 |
| Hippocampus | 0.67 ± 0.04 | 5.85 ± 0.84 | 0.71 ± 0.04 | 5.62 ± 0.77 |
| Thalamus | 0.47 ± 0.10 | 6.90 ± 1.05 | 0.74 ± 0.04 | 6.93 ± 1.22 |
| Hypothalamus | 0.95 ± 0.28 | 5.66 ± 0.68 | 1.04 ± 0.13 | 5.35 ± 0.86 |
| Striatum | 0.70 ± 0.06 | 5.59 ± 0.75 | 0.80 ± 0.04 | 5.63 ± 0.85 |
| Pallidum | 0.85 ± 0.09 | 5.43 ± 0.65 | 0.80 ± 0.04 | 5.41 ± 0.88 |
| Olfactory Bulb | 0.76 ± 0.16 | 5.47 ± 0.67 | 1.23 ± 0.10 | 5.58 ± 1.04 |
| Corpus Callosum | 0.70 ± 0.05 | 6.05 ± 0.95 | 0.77 ± 0.06 | 6.09 ± 0.96 |
| White Matter | 0.83 ± 0.11 | 6.01 ± 0.85 | 0.95 ± 0.06 | 5.89 ± 0.83 |
| Ventricles | 1.39 ± 0.30 | 6.47 ± 0.96 | 1.48 ± 0.12 | 6.70 ± 1.50 |
| **Whole brain** | **0.73 ± 0.03** | **5.57 ± 0.77** | **0.76 ± 0.03** | **5.45 ± 0.75** |

**Table S1.** Values corresponding to regional brain distribution of $^{64}$Cu uptake (%ID/mL) in 6-8-month-old C57BL6J mice at 30 min and 24 h post-injection of $^{64}$Cu-acetate (green) and $^{64}$Cu-GTSM (blue). Data are mean (n=4 for $^{64}$Cu-acetate mice; n=6 for $^{64}$Cu-GTSM) ± SD, with %ID/g resulting from the InviCRO brain atlas applied to the PET datasets. These values of %ID/g correspond to the sum of activity (MBq) within each brain region divided by the sum of activity (MBq) of the whole body (excluding tail).

**Brain Biodistribution of $^{64}$Cu-Acetate and $^{64}$Cu-GTSM: One-way ANOVA Analysis on %ID/g of Individual Brain Regions**

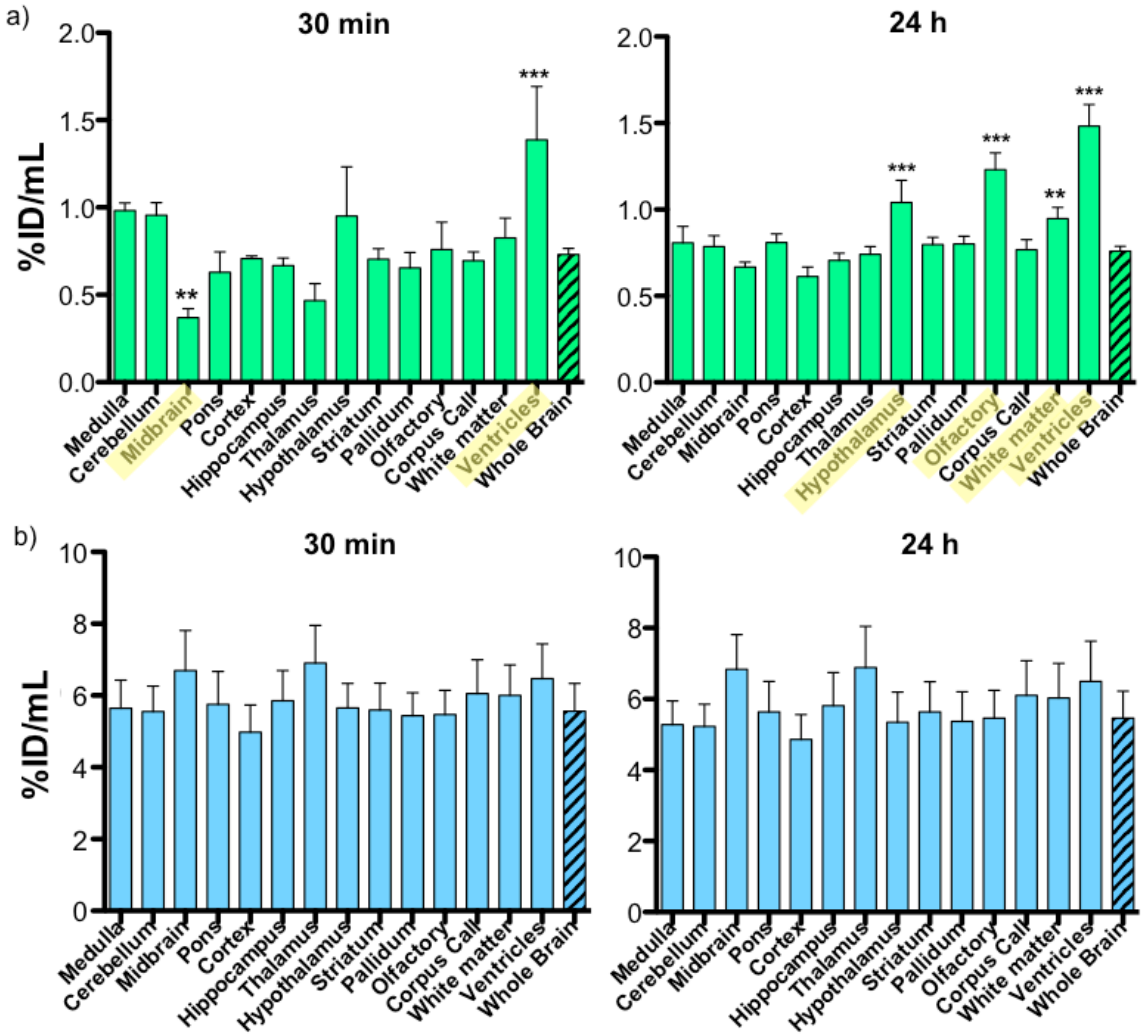


**Fig. S5**. (a) Left: One-way ANOVA analyses of %ID/g (including Dunnett's multiple comparison post-hoc tests) confirm significantly lower %ID/g in the midbrain vs. whole brain (*p*-value <0.01, F=13.39) and significantly higher %ID/g in the ventricles vs. whole brain (*p*-value <0.001, F=13.39) for $^{64}$Cu-acetate at 30 min; Right: the same analysis at 24 h, showing significantly higher %ID/g in the hypothalamus (*p*-value <0.0001, F=41.29), olfactory bulb (*p*-value <0.0001, F=41.29), white matter (*p*-value <0.001, F=41.29), and ventricles (*p*-value <0.0001, F=41.29) vs. whole brain at 24 h. Data are mean (n=4) ± SD, with %ID/g resulting from the InviCRO brain atlas applied to the PET datasets. (b) A one-way ANOVA with Dunnett's multiple comparison post-hoc tests for $^{64}$Cu-GTSM confirms no differences of %ID/g in any of the individual brain regions compared to whole brain. Data are mean (n=6) ± SD, with %ID/g resulting from the InviCRO brain atlas applied to the PET datasets.

One-way ANOVA analyses of %ID/mL (including Dunnett's multiple comparison post-hoc tests) confirm significantly lower %ID/mL in the midbrain vs. whole brain (*p*-value <0.01, F=13.39) and significantly higher %ID/g in the ventricles vs. whole brain (*p*-value <0.001, F=13.39) for $^{64}$Cu-acetate at 30 min; the same analysis and significantly higher %ID/g in the hypothalamus (*p*-

value <0.0001, F=41.29), olfactory bulb (*p*-value <0.0001, F=41.29), white matter (*p*-value <0.001, F=41.29), and ventricles (*p*-value <0.0001, F=41.29) vs. whole brain at 24 h.

**Focal Accumulation of $^{64}$Cu in the Ventricles of all the $^{64}$Cu-Acetate Mice**

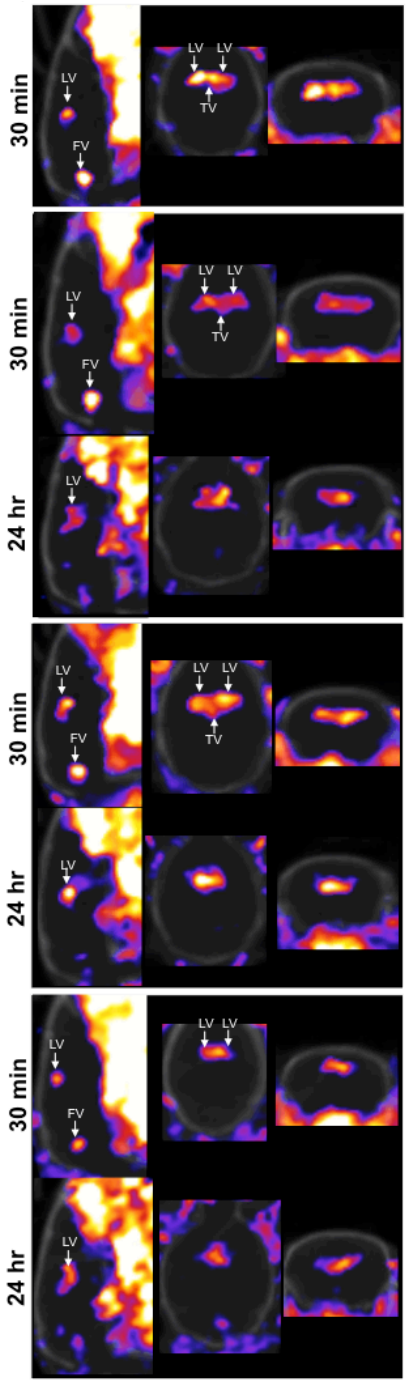


**Fig. S6**. Representative coronal and sagittal slices though all PET/CT images corresponding to the $^{64}$Cu-acetate from 4 different mice at 30 min and 24 h post injection. Prominent focal accumulations of $^{64}$Cu signal are observed in/around the lateral ventricles (LV), third ventricles (TV), and fourth ventricles (FV) at 30 min, with the FV signal attenuating somewhat by 24 h.

Statistical analysis of the autoradiographic images using one-way ANOVA with Dunnett's multiple comparison post-hoc tests confirm significantly higher ROI:WB phosphor density ratio in the lateral (L) ventricles (*p*-value <0.0001, F=64.13), fimbria (*p*-value <0.0001, F=64.13), corpus callosum (*p*-value <0.05, F=64.13), caudate putamen (*p*-value <0.05, F=64.13), and

hypothalamus (*p*-value <0.0001, F=64.13) compared to olfactory bulb, the region with least signal (right). Additional one-way ANOVA with Dunnett's multiple comparison post-hoc tests confirm significantly higher ROI:OB phosphor density ratio in the lateral (L) ventricles (*p*-value <0.0001, F=38.20) vs. OB, fimbria (*p*-value <0.0001, F=38.20) vs. OB, and hypothalamus (*p*-value <0.001, F=38.20) compared to (OB). It was not, however, possible to definitively identify whether the ventricular space (cerebrospinal fluid, CSF), the choroid plexus or the hippocampal fimbria, or a combination of these, was the most radioactive anatomical structure.

**Clearance from brain after administration of $^{64}$Cu-acetate by PET**

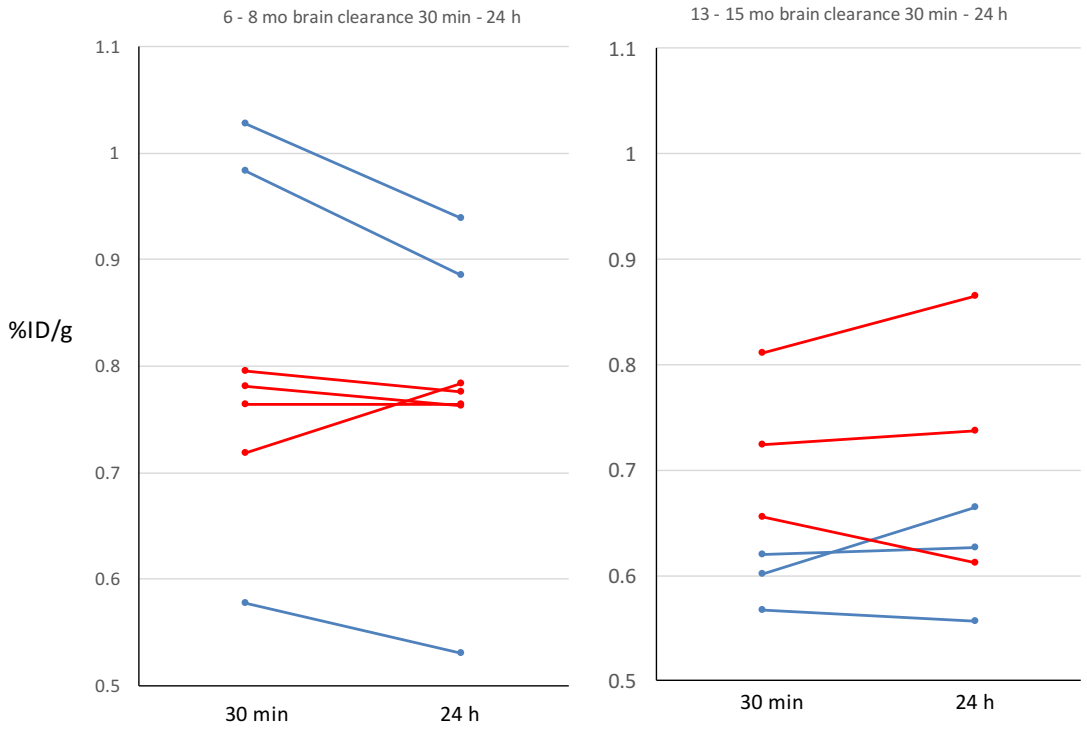


**Fig. S7**. %ID/g in brains of individual mice at 30 and 24 h, measured by quantitative PET. left, 6-8 month old mice; right, 13-15 month old mice. Blue line: TASTPM mice; red line: wild type mice. Only the 6-8 month old TASTPM mice show significant clearance of activity from brain between 30 min and 24 h.